Published in final edited form as:
Neuroscience. 2010 September 15; 169(4): 1651–1661. doi:10.1016/j.neuroscience.2010.06.011.

Relationship of Cannabinoid CB1 Receptor and Cholecystokinin Immunoreactivity in Monkey Dorsolateral Prefrontal Cortex

Stephen M. Eggan[1], **Darlene S. Melchitzky**[1,2], **Susan R. Sesack**[1,3], **Kenneth N. Fish**[1], and **David A. Lewis**[1,3]

[1] Department of Psychiatry, University of Pittsburgh, Pittsburgh, PA 15213

[2] Department of Biology, Mercyhurst College, Erie, PA 16546

[3] Department of Neuroscience, University of Pittsburgh, Pittsburgh, PA 15260

Abstract

Exposure to cannabis impairs cognitive functions reliant on the circuitry of the dorsolateral prefrontal cortex (DLPFC) and increases the risk of schizophrenia. The actions of cannabis are mediated via the brain cannabinoid 1 receptor (CB1R), which in rodents is heavily localized to the axon terminals of cortical GABA basket neurons that contain cholecystokinin (CCK). Differences in the laminar distribution of CB1R-immunoreactive (IR) axons have been reported between rodent and monkey neocortex, suggesting that the cell type(s) containing CB1Rs, and the synaptic targets of CB1R-IR axon terminals, may differ across species; however, neither the relationship of CB1Rs to CCK-containing interneurons, nor the postsynaptic targets of CB1R and CCK axon terminals, have been examined in primate DLPFC. Consequently, we compared the distribution patterns of CB1R- and CCK-IR structures, determined the proportions of CB1R and CCK neurons that were dual-labeled, and identified the synaptic types and postsynaptic targets of CB1R- and CCK-IR axon terminals in macaque monkey DLPFC. By light microscopy, CB1R- and CCK-IR axons exhibited a similar laminar distribution, with their greatest densities in layer 4. Dual-label fluorescence experiments demonstrated that 91% of CB1R-IR neurons were immunopositive for CCK, whereas only 51% of CCK-IR neurons were immunopositive for CB1R. By electron microscopy, all synapses formed by CB1R-IR axon terminals were symmetric, whereas CCK-IR axon terminals formed both symmetric (88%) and asymmetric (12%) synapses. The primary postsynaptic target of both CB1R- and CCK-IR axon terminals forming symmetric synapses was dendritic shafts (81–88%), with the remainder targeting cell bodies or dendritic spines. Thus, despite species differences in laminar distribution, CB1Rs are principally localized to CCK basket neuron axons in both rodent neocortex and monkey DLPFC. These axons target the perisomatic region of pyramidal neurons, providing a potential anatomical substrate for the impaired function of the DLPFC associated with cannabis use and schizophrenia.

Corresponding author: Stephen M. Eggan, PhD, Department of Psychiatry, University of Pittsburgh, 3811 O'Hara Street, W1651 BST, Pittsburgh, PA 15213, Phone: (412) 624-3934, Fax: (412) 624-9910, eggansm@upmc.edu.

DISCLOSURE/CONFLICTS OF INTEREST

David A. Lewis currently receives investigator-initiated research support from the BMS Foundation, Bristol-Myers Squibb, Curridium Ltd and Pfizer and in 2007–2009 served as a consultant in the areas of target identification and validation and new compound development to AstraZeneca, BioLine RX, Bristol-Myers Squibb, Hoffman-Roche, Lilly, Merck, Neurogen and SK Life Science. All other authors declare that, except for income received from their primary employer, no financial support or compensation has been received from any individual or corporate entity over the past three years for research or professional service and there are no personal financial holdings that could be perceived as constituting a potential conflict of interest.

Keywords

Cannabis; GABA; parvalbumin; primate; schizophrenia; working memory

INTRODUCTION

In both humans and animals, exposure to marijuana and other forms of cannabis produces impairments in cognitive functions including those subserved by the dorsolateral prefrontal cortex (DLPFC), such as working memory (Winsauer et al., 1999; Schneider and Koch, 2003; D'Souza et al., 2004). In addition, cannabis use, particularly during adolescence, represents a significant risk factor for the later appearance of schizophrenia (Henquet et al., 2005; Moore et al., 2007), a disorder characterized by both dysfunction of the DLPFC and working memory impairments (Lewis et al., 2005). The effects of cannabis are mediated principally by the cannabinoid 1 receptor (CB1R) (Freund et al., 2003), which in the primate neocortex is heavily expressed in the DLPFC (Eggan and Lewis, 2007).

In primates, working memory function depends critically on the synaptic connectivity and patterns of activity within the DLPFC (Goldman-Rakic, 1995). In particular, networks of interconnected GABA interneurons are essential for the synchronization of neural networks (Connors and Long, 2004) in the oscillatory patterns required for working memory (Howard et al., 2003). Consistent with these findings, working memory performance in monkeys is disrupted by $GABA_A$ receptor antagonists injected into the DLPFC (Sawaguchi et al., 1988; Rao et al., 2000).

In the rodent neocortex, CB1Rs are to a minor extent contained in excitatory synapses and modulate glutamate release (Kawamura et al., 2006; Katona et al., 2006); however, the CB1R is most heavily expressed by, and localized to the axon terminals of, the subtype of GABA basket interneurons that contain the neuropeptide cholecystokinin (CCK) and target the cell bodies and apical dendrites of pyramidal neurons (Katona et al., 1999; Marsicano and Lutz, 1999; Bodor et al., 2005). In line with this anatomical localization, activation of CB1Rs by either exogenous or endogenous cannabinoids inhibits the release of GABA from CCK terminals and strongly suppresses $GABA_A$ receptor-mediated inhibitory postsynaptic currents in pyramidal neurons (Trettel et al., 2004; Galarreta et al., 2004; Bodor et al., 2005). In the rodent hippocampus, CB1R activation promotes the activation of signaling cascades that stimulate the translation of proteins involved in neuronal development and long-term modification of synaptic strength by altering the balance of inhibitory and excitatory tone (Puighermanal et al., 2009). Furthermore, in the rodent neocortex, CB1R/CCK-containing neurons are electrically coupled and entrain oscillatory patterns of network activity (Galarreta et al., 2004; Klausberger et al., 2005; Robbe et al., 2006), which are disrupted following administration of CB1R agonists (Robbe et al., 2006; Hajos et al., 2008).

In concert, these data from rodent suggest that if CB1Rs are contained in CCK neurons in the human DLPFC, then alterations in CB1R signaling in schizophrenia could contribute to the altered cortical circuitry and impaired network oscillations associated with working memory impairments in the illness. However, rodent-primate species differences appear to be present in the laminar distribution of CB1R-containing axons in frontal and somatosensory cortices (Glass et al., 1997; Egertová and Elphick, 2000; Bodor et al., 2005; Eggan and Lewis, 2007). Furthermore, species-dependent differences in CB1R ligand binding levels and in the relative sensitivity of GABA suppression to CB1R agonists are reported across rodents (Hungund and Basavarajappa, 2000; Haller et al., 2007). These findings raise the possibility that CB1Rs may be expressed by different GABA neuron populations across different species and that in the primate neocortex CB1R- and CCK-

containing axon terminals may have different postsynaptic targets from those previously reported in rodents (Katona et al., 1999; Bodor et al., 2005).

In the primate DLPFC, CB1Rs are preferentially contained in cells and axon terminals that have morphologic features characteristic of GABA neurons (Eggan and Lewis, 2007); however, neither the colocalization of CB1Rs and CCK in cortical structures, nor the synaptic targets of CB1R- and CCK-containing axon terminals have been examined. Consequently, in this study we used immunocytochemistry and light and electron microscopy to 1) determine whether CB1R and CCK immunoreactivities are colocalized in cell bodies and axon terminals; 2) determine the proportions of CB1R- and CCK dual-labeled neurons; 3) identify the type(s) of synapses formed by, and the synaptic targets of, CB1R- and CCK-immunoreactive (IR) axon terminals; and 4) determine whether these targets differ as a function of cortical layer in monkey DLPFC area 46.

EXPERIMENTAL PROCEDURES

Light Microscopy

Animals and Tissue Preparation—For light microscopy studies, four adult (4.3–6.3 kg), male, long-tailed macaque monkeys (*Macaca fascicularis*) were utilized. Monkeys were deeply anesthetized with 25 mg/kg ketamine hydrochloride and 30 mg/kg sodium pentobarbital and then perfused transcardially with ice-cold 1% paraformaldehyde in 0.1 M phosphate buffer (PB; pH 7.4) followed by 4% paraformaldehyde in PB, as previously described (Oeth and Lewis, 1993). Brains were immediately removed and coronal blocks (5–6 mm-thick) were postfixed in phosphate-buffered 4% paraformaldehyde at 4°C for 6 hours. Tissue blocks were subsequently cryoprotected and then stored at −30°C as previously described (Oeth and Lewis, 1993). We have previously shown that immunoreactivity for a number of antigens are unaffected by this storage procedure [see (Cruz et al., 2003)]. Coronal blocks containing DLPFC area 46 from either the left or the right hemisphere were sectioned at 40 μm on a cryostat and every 10^{th} section was stained for Nissl substance with thionin.

Housing and experimental procedures were conducted in accordance with guidelines set by the United States Department of Agriculture and the National Institutes of Health *Guide for the Care and Use of Laboratory Animals* and with approval of the University of Pittsburgh's Institutional Animal Care and Use Committee.

Immunocytochemistry and dual-label immunofluorescence—For standard single-label immunocytochemistry, free-floating coronal tissue sections containing DLPFC area 46 were processed as previously described (Eggan and Lewis, 2007). Briefly, tissue sections were immersed in a blocking solution for 30 min to reduce background labeling, and then incubated at 4°C for 48 hours in blocking solution containing an affinity-purified polyclonal guinea pig anti-CB1R antibody raised against the entire C-terminus of the rat CB1R (diluted 1:4000; generously provided by Dr. Ken Mackie, Indiana University, Bloomington, IN), or a monoclonal mouse anti-CCK antibody raised against gastrin (diluted 1:4000; antibody #9303 provided by the CURE Digestive Diseases Research Center, Antibody/RIA Core, Los Angeles, CA, NIH Grant DK41301). Sections were then incubated in blocking solutions containing either biotinylated donkey, anti-guinea pig, or anti-mouse IgG secondary antibody (diluted 1:200; Jackson ImmunoResearch, West Grove, PA) and processed with the avidin-biotin-peroxidase method (Hsu et al., 1981) using the Vectastain Avidin-Biotin Elite Kit (Vector Laboratories, Burlingame, CA). The immunoperoxidase reaction was visualized using 3,3′-diaminobenzidine (DAB; 0.005%; Sigma, St. Louis, MO). The DAB reaction product was stabilized by serial immersion of slide-mounted sections in osmium tetroxide (0.005%) and thiocarbohydrazide (0.5%) (Lewis et al., 1986). All incubations and washes

were performed on a shaker at room temperature (RT) except for the primary antibody incubation.

For dual-label immunofluorescence experiments, free floating coronal tissue sections were pretreated in a blocking solution containing 0.3% Triton X-100, 5% normal goat serum (NGS) or normal donkey serum (NDS) and normal human serum (NHuS), 1% BSA, 0.1% glycine, and 0.1% lysine in phosphate buffered saline (PBS; used in all antibody solutions) at RT for 3 hours to reduce background. Sections were then incubated at 4°C for 48 hours in the same blocking solution containing the guinea pig anti-CB1R antibody (diluted 1:3000) or an affinity-purified polyclonal rabbit anti-CB1R antibody raised against the last 15 amino acid residues of the rat CB1R (diluted 1:5000; generously provided by Dr. Ken Mackie, Department of Psychological and Brain Sciences and Program in Neuroscience, Indiana University, Bloomington, IN) and either the monoclonal mouse anti-CCK antibody (diluted 1:2000) or a monoclonal mouse IgG1 antibody against parvalbumin (PV; diluted 1:8000; Swant, Bellinzona, Switzerland). Sections were then washed in PBS and incubated for 24 hours in blocking solution containing an anti-rabbit Alexa 488 secondary antibody (Invitrogen, Carlsbad, CA) to visualize the CB1R antibody and an anti-mouse indocarbocyanine (Cy3; Jackson) conjugated secondary antibody to visualize the CCK antibody (both raised in donkey; diluted 1:500). Additional experiments were performed using an anti-guinea pig Alexa 633 secondary antibody to visualize the CB1R antibody and an anti-mouse Alexa 488 secondary antibody (both raised in goat; diluted 1:500; Invitrogen) to visualize the CCK and PV antibodies. Sections were subsequently mounted on gel-coated slides, and coverslips applied with Vectashield (Vector).

Fluorescent images were collected on an Olympus BX51 microscope fitted with an Olympus DSU spinning disk confocal (Olympus America Inc., Melville, NY), a Hamamatsu C4742-98 CCD camera (Hamamatsu Corporation, Bridgewater, NJ), and a Ludl motorized XYZ stage (LEP Ltd., Hawthorne, NY). Images were captured using a 60X 1.42 NA plan apochromat N objective or a 40X 1.3 plan fluorite objective. Qualitative images were deconvolved using Intelligent Imaging Innovations' constrained iterative algorithm in Slidebook 4.2 (Denver, CO). Images are projected images of sequential confocal z-plane sections taken 0.22–0.5 μm apart. Semi-quantitative analysis was performed in DLPFC area 46 on non-deconvolved image stacks in Slidebook 4.2 (Denver, CO) by optimally adjusting background and brightness in the green and red channels for each image stack, independently marking CB1R- or CCK-IR neurons in either the green (CB1R) or red (CCK) channel across each z-plane, and then quantifying the number of single- or dual-labeled neurons in overlay images. Because the levels of CB1R immunoreactivity in cell bodies is lower than those for CCK, all CB1R-IR neurons were identified first and CCK-IR neurons were identified second, in order to reduce bias. Two sections from each of three animals were quantified. Across all animals, a total of 887 CB1R-IR and 1479 CCK-IR neurons were identified.

Electron Microscopy

Animals and Tissue Preparation—For electron microscopy studies, three additional adult (3.1–6.2 kg), male, long-tailed macaque monkeys were perfused as described above except that the perfusate was room temperature 1% paraformaldehyde and 0.05% glutaraldehyde in 0.1 M PB followed by 4% paraformaldehyde and 0.2% glutaraldehyde in 0.1 M PB as previously reported (Melchitzky et al., 2005). Brains were immediately removed and coronal blocks (5-mm-thick) were immersed in phosphate buffered 4% paraformaldehyde at 4°C for 2 hours. Coronal tissue blocks containing DLPFC area 46 were washed several times in 0.1 M PB and sectioned at 50 μm on a vibrating microtome.

Immunocytochemistry—To improve antigenicity and reduce nonspecific immunoreactivity, free-floating tissue sections containing DLPFC area 46 were initially treated with 1% sodium borohydride in 0.1 M PB for 30 min, washed extensively in 0.1 M PB, and then incubated in a blocking solution containing 0.2% BSA, 0.04% Triton X-100, 3% NDS, and 3% NHuS in 0.01 M PBS for 30 min as previously described (Sesack et al., 1998). Sections from each animal were subsequently incubated overnight in blocking solution containing either the rabbit anti-CB1R antibody (diluted 1:5000) or the monoclonal mouse anti-CCK antibody (diluted 1:2000 or 1:1500). On the following day, sections were rinsed in PBS and incubated for 1 hour in blocking solution containing either a biotinylated anti-rabbit or anti-mouse IgG secondary antibody made in donkey (diluted 1:200; Jackson). Following rinses in PBS, sections were processed with the avidin-biotin-peroxidase method and visualized with DAB as described above, postfixed in 2% osmium tetroxide for 1 hour and embedded in Epon 812 (EM bed 812; Electron Microscopy Sciences, Fort Washington, PA) as previously described (Sesack et al., 1995).

Sampling Regions and Procedures—For each animal and each primary antibody condition, separate trapezoid blocks from two tissue sections were cut from layers 2-superficial 3 (2–3s) and layer 4 in DLPFC area 46 (Fig. 1A). Trapezoid blocks were sectioned on a Reichert ultramicrotome (Nussloch, Germany) at 80 nm and two to four ultrathin sections were serially collected on 200- or 400-mesh copper grids and counterstained with uranyl acetate and lead citrate. For each trapezoid block 1–2 grids, separated by at least 10 grids, were examined on a FEI Morgagni transmission microscope (Hillsboro, OR). One section per grid was arbitrarily chosen as the starting point for analysis and within each selected section all CB1R- or CCK-labeled structures were captured and stored for later analysis. All labeled axon terminals were identified, photographed at X22,000, and classified according to their synaptic specialization and appositional or postsynaptic target.

Identification of Neuronal and Synaptic Elements—Neuronal elements encountered in electron micrographs were identified according to previous descriptions (Peters et al., 1991). Axon terminals were identified by the presence of small vesicles and often contained mitochondria. Axon terminals forming asymmetric synapses (Gray's type I) were distinguished by the widening and parallel spacing of apposed plasmalemmal surfaces and small round synaptic vesicles. In addition, asymmetric synapses were identified by the presence of a prominent postsynaptic density. In contrast, axon terminals forming symmetric synapses (Gray's type II) were identified by the presence of intercleft filaments, pleomorphic small synaptic vesicles, and a thin postsynaptic density. The presence of a nucleus identified somata. Dendritic shafts were identified by the presence of postsynaptic specializations, mitochondria, microtubules, and neurofilaments. Dendritic spines were characterized by the absence of both organelles and microtubules.

Antibody Specificity

The specificity of the rabbit anti-CB1R antibody has been previously demonstrated by several lines of evidence including preadsorption experiments and Western blot analysis (Eggan and Lewis, 2007). In addition, we tested the specificity of the rabbit anti-CB1R antibody in fixed tissue from CB1R knockout mice (generously provided by Nestor Barrezueta, Bristol Myers-Squibb); CB1R immunoreactivity was completely absent in CB1R knockout mice (Supplementary Fig. S1). Although CB1R immunoreactivity has been observed in both asymmetric, excitatory synapses and symmetric, inhibitory synapses in the neocortex (Kawamura et al., 2006; Katona et al., 2006), the antibody utilized in the present study exclusively labels symmetric, inhibitory synapses by electron microscopy in both the rodent hippocampus (Katona et al., 1999; Hajos et al., 2000) and monkey DLPFC (Eggan

and Lewis, 2007), probably because the level of CB1Rs in excitatory terminals is below the threshold of detectability (Katona et al., 2006; Eggan and Lewis, 2007). Hence, the findings of this study relate specifically to CB1R immunoreactivity in inhibitory neurons and axon terminals. The specificity of the guinea pig anti-CB1R antibody has also been confirmed by testing in tissue from CB1R knockout mice (K. Mackie, Department of Psychological and Brain Sciences and Program in Neuroscience, Indiana University, personal communication). The mouse monoclonal anti-CCK antibody was raised against gastrin, but recognizes CCK due to a homologous terminal pentapeptide shared by gastrin and CCK. Gastrin is not present in the neocortex (Rehfeld, 1978; Geola et al., 1981); thus, only CCK was detected in this study. The specificity of the anti-CCK antibody has been demonstrated by its high affinity for the CCK peptide (Kovacs et al., 1989), by preadsorption experiments in monkey tissue (Oeth and Lewis, 1990), and by experiments in which an excess of antigen added to the incubation serum produced no labeling (Hefft and Jonas, 2005). The specificity of the PV antibody has been previously demonstrated (Celio et al., 1988) and has been used in multiple studies (DeFelipe et al., 1999; Cruz et al., 2003).

Statistical Analyses

Individual 2×3 or 2×2 χ^2 analyses were performed to compare laminar differences in the relative proportions of postsynaptic targets of CB1R or CCK-IR axon terminals forming symmetric synapses. Individual 2×3 or 2×2 χ^2 analyses were also performed to compare the differences in the relative proportions of postsynaptic targets of CB1R and CCK-IR postsynaptic targets within layers.

Photography

Brightfield photomicrographs were obtained with a Zeiss Axiocam camera. Digital electron micrographs images were captured using an AMT XP-60 digital camera (Danvers, MA). Brightfield photomontages and digital electron micrographs were assembled, and the brightness and contrast were adjusted in Adobe Photoshop. Immunofluorescent images were obtained and assembled as described earlier.

RESULTS

General Observations

The localization and laminar distribution patterns of immunoreactivity produced by the guinea pig anti-CB1R and mouse anti-CCK antibodies were identical to those previously described in the monkey DLPFC (Fig. 1) (Oeth and Lewis, 1993;Eggan and Lewis, 2007). Comparison of CB1R and CCK immunoreactivities revealed very similar patterns of labeled structures and laminar distributions. Both CB1R- and CCK-IR neurons had either a vertically oriented oval cell body or a large multipolar somal morphology (Fig. 2A, C) and were present in highest number in layers 2–3s (Fig. 1). However, the density of CB1R-IR neurons was relatively lower compared to the density of CCK-IR neurons (Fig. 1B, C). CB1R- and CCK-IR axons exhibited a distinctive laminar innervation pattern with layers 4 and 6 containing dense bands of axons and varicosities (Fig. 1). CB1R- and CCK-IR axons were observed to form “baskets” around unlabeled cell bodies (Fig. 2B, D). However, in contrast to CB1R-IR axons, the densities of CCK-IR axons and varicosities were relatively lower in each cortical layer (Fig. 1B, C), and the intervaricose segments were less distinct (Fig. 2). Thus, while CB1R-IR axons and varicosities resembled “pearls on a string,” CCK-IR profiles had a punctate appearance (Fig. 2).

Analysis of dual-labeled tissue

CB1R and CCK labeling was frequently colocalized in axons and varicosities (Fig. 3D-F); however, both CB1R and CCK single-labeled axons and axon varicosities were also observed. CB1R/CCK-IR axons frequently formed perisomatic arrays around unlabeled cell bodies. In layers 2–3, most CB1R-IR neurons were also CCK-IR (Fig. 3A-C); however, many CCK-IR neurons were CB1R immunonegative. Across all monkeys counted, a mean (±SD) 90.6 ± 3.7% of CB1R-IR neurons were CCK-IR, whereas only 50.7 ± 14.6% of CCK-IR cells were CB1R-IR.

In contrast, CB1R immunoreactivity was never observed in PV labeled structures (Supplementary Fig. S2). Even at the border of layers 3 and 4, where the density of both CB1R- and PV-IR axons is highest in monkey area 46, axons and varicosities were always single-labeled for either CB1R or PV (Supplementary Fig. S2). However, CB1R- and PV-IR single-labeled axons did form perisomatic arrays around the same unlabeled cell bodies (Supplementary Fig. S2).

Synapses formed by, and postsynaptic targets of, CB1R- or CCK-IR axon terminals

Of 111 CB1R-IR axon terminals with an identifiable synaptic specialization, all formed classic symmetric synapses; 98% were onto small or large unlabeled dendritic shafts (Fig. 4A, D), dendritic spines (Fig. 4C), or somata. Some dendritic shafts that were contacted by CB1R-IR axon terminals exhibited morphologic characteristics of interneuron dendrites, such as a varicose shape and a high density of synapses (data not shown) (McGuire et al., 1991; Smiley and Goldman-Rakic, 1993); however, most contacted dendritic shafts were cut in cross-section, precluding the identification of the neuron type of origin. In addition, a small number (2%) of CB1R-IR axon terminals formed symmetric synapses onto CB1R-IR dendrites (Fig 4B). Occasionally, CB1R-IR axons were found to form multiple appositions around unlabeled pyramidal cell bodies (Fig. 4E).

Of 95 CCK-IR axon terminals with identifiable synaptic specializations, 88% formed symmetric synapses that targeted large or small unlabeled dendritic shafts (Fig. 5A, B), dendritic spines (Fig. 5C), or somata (Fig. 5D). Some dendritic shafts contacted by CCK-IR axon terminals were varicose in shape and received other synaptic inputs (Fig. 6A, B), consistent with an origin from non-pyramidal neurons. The remaining 12% of CCK-IR axon terminals formed classic asymmetric synapses primarily onto spines (Fig. 6B) and to a lesser extent onto unlabeled dendritic shafts (Fig. 6A).

Laminar analysis of CB1R or CCK-IR axon terminal postsynaptic targets

No significant laminar differences were present in the postsynaptic targets of CB1R-IR terminals that had an identifiable synaptic specialization ($\chi^2 = 2.34$, $P = 0.311$, $df = 2$; Table 1). In both layers 2–3s and layer 4, the majority of symmetric synapses were onto dendritic shafts (88% and 87%, respectively; Table 1). In addition, the smaller proportions of symmetric synapses onto dendritic spines and somata were similar in both layers (Table 1). Consistent with these observations, most CB1R-IR appositions (n = 340; axon terminals without identifiable synapses, but that would presumably form a synapse in another plane of section) were with dendritic shafts in both layer 2–3s (90%) and layer 4 (85%), with smaller proportions associated with spines (7% in layer 2–3s; 5% in layer 4) and somata (3% in layer 2–3s; 10% in layer 4).

CCK-IR terminals showed no significant differences in postsynaptic targets by layer ($\chi^2 = 2.54$, $P = 0.280$, $df = 2$; Table 1). The major postsynaptic target of CCK-IR axon terminals forming symmetric synapses was dendritic shafts in both layers 2–3s (81%) and layer 4 (83%). Likewise, CCK-IR axon terminal appositions (n = 185) were also predominantly

with dendritic shafts in both layer 2–3s (90%) and layer 4 (85%), with smaller proportions associated with spines (9% in both layers 2–3s and 4) and somata (6% in layer 2–3s; 8% in layer 4).

The postsynaptic targets of CB1R- and CCK-IR symmetric synapses did not significantly differ in layer 4 ($\chi^2 = 0.56$, $P = 0.755$, $df = 2$; Table 1). In contrast, the postsynaptic targets of CB1R- and CCK-IR symmetric synapses in layers 2–3s were significantly different ($\chi^2 = 6.93$, $P = 0.031$, $df = 2$; Table 1), apparently due primarily to a larger proportion of CCK-IR symmetric synapses targeting somata (11%) than CB1R-IR symmetric synapses (0%).

DISCUSSION

The results of this study demonstrate that in macaque monkey DLPFC area 46 1) the morphology and the laminar distributions of CB1R- and CCK-IR neurons and axons are very similar; 2) CB1R and CCK labeling is colocalized in neurons, axons, and axon terminals, although structures single-labeled for each protein are also present; 3) Most CB1R-IR neurons are CCK-IR, whereas only half of CCK-IR neurons are CB1R-IR; 4) CB1R-IR axon terminals exclusively form symmetric synapses, whereas CCK-IR axon terminals form both symmetric and asymmetric synapses; 5) The majority of both CB1R- and CCK-IR axon terminals forming symmetric synapses contact dendritic shafts; and 6) The synaptic targets of CB1R- and CCK-IR axon terminals are similar in layer 4, but different in layers 2–3s, where CCK-IR terminals are more likely to contact cell bodies and less likely to contact spines than are CB1R-IR terminals.

Sources of CB1R and CCK-IR axon terminals

In the rodent, it is well established that CB1Rs are predominantly expressed by, and localized to the terminals of, a subset of CCK-containing GABA basket neurons. However, comparison of findings across primate and rodent studies reveal differences in the laminar distribution of CB1R-IR axons in frontal and somatosensory cortices (Katona et al., 1999; Bodor et al., 2005). For example, in rat frontal cortex CB1R-IR axons are most dense in layers 2–3 and 6 and least dense in layer 4 (Egertová and Elphick, 2000), whereas layer 4 contains the highest density of CB1R-IR axons in monkey and human prefrontal cortex (Eggan and Lewis, 2007). Furthermore, the rat somatosensory cortex contains a dense band of CB1R-IR axons in layer 5A, bordered by sparse axon labeling in layers 4 and 5B (Bodor et al., 2005). In contrast, in the monkey primary somatosensory cortex the density of axons is relatively similar across layers 2–3 and 5–6, with sparse axonal labeling in layer 4 (Eggan and Lewis, 2007). These findings indicate that within homologous cortical regions, primates and rodents differ in the laminar distribution of CB1R-IR axons, suggesting that CB1Rs may be expressed by different GABA neuron populations across species that have different postsynaptic targets.

However, the findings of this study, consistent with those in the rodent, indicate that the source of the axons immunoreactive for CB1Rs is most likely intrinsic CCK inhibitory basket interneurons. This idea is supported by the presence of CB1R and CCK labeling in somata and terminals with the morphological features of GABA neurons and the colocalization of CB1R and CCK labeling in neurons across layers 2–3. Indeed, the proportions of CB1R and CCK neurons that were dual-labeled in this study are similar to those reported in the rodent neocortex (Marsicano and Lutz, 1999; Bodor et al., 2005). In both the monkey and human DLPFC, layers 2–3 contain the highest density of CB1R and CCK immunoreactive and mRNA-expressing neurons (Hendry et al., 1983; Eggan et al., 2008; Hashimoto et al., 2008), whereas the highest densities of CB1R- and CCK-IR axons and terminals are present in layer 4. This difference in the laminar distribution of immunoreactive neurons and axons may be explained by previous studies in monkey

DLPFC demonstrating that the axons of CCK-containing neurons in layers 2–3 project radially into, and collateralize within, layer 4 (Lund and Lewis, 1993). Thus, the presence of interneurons in superficial layers that express both CB1Rs and CCK could account for the colocalization of these proteins and the similar postsynaptic targets of CB1R- and CCK-IR axon terminals in layer 4.

In the rodent neocortex, two distinct populations of CCK-containing cells have been identified: Small bipolar CCK-IR neurons often contain calretinin (CR), whereas large, multipolar CCK-IR neurons lack this calcium binding protein (Kubota and Kawaguchi, 1997). In addition, CB1R-IR neurons in the rat cortex contain either CCK or the calcium binding protein calbindin (Bodor et al., 2005). Based upon these findings, the CCK-positive, CB1R-negative axons and terminals observed in the monkey DLPFC in this study likely arise from CR-containing GABA neurons, whereas the CCK-negative, CB1R-positive axons and terminals likely arise from calbindin-containing GABA neurons. CCK/CR-containing and CB1R/calbindin-containing neurons could be the source the of CCK-IR or CB1R-IR inhibitory synaptic inputs to dendritic spines or shafts of pyramidal neurons or to dendrites of GABA interneurons and thus might serve to influence incoming excitatory input to pyramidal neurons as well as mediating overall network disinhibition (Zaitsev et al., 2005). In addition, CB1R-IR terminals were also found to synapse onto CB1R-IR dendrites, which could serve to regulate other CB1R-IR neurons or may allow CB1R-IR neurons to self-inhibit themselves through autaptic synapses (Bacci et al., 2004). These different sources of CB1R- and CCK-IR axons remain to be determined in the monkey DLPFC, but may account for the single-labeled CB1R and CCK neuron populations and for the different synaptic targets of CB1R- and CCK-IR axons in layers 2–3s.

In contrast to our findings of CB1R immunoreactivity exclusively in terminals forming symmetric synapses, two recent studies using a well–characterized anti-CB1R antibody raised against the C-terminus (amino acid residues 443–473) of the rat CB1R reported asymmetric synapses formed by CB1R-IR axon terminals in the rat hippocampus, suggesting that CB1Rs are also located in excitatory terminals that release glutamate (Kawamura et al., 2006; Katona et al., 2006). Because this CB1R antibody and the ones used in the present study both meet the “gold standard” of antibody specificity (Saper and Sawchenko, 2003; Saper, 2005), the differences in findings across studies are more likely to represent differences in antibody sensitivity than specificity. Consistent with this interpretation, use of semi-quantitative immunogold electron microscopy (Kawamura et al., 2006), revealed that the density of CB1Rs is 20- to 30-fold higher in inhibitory terminals than in excitatory terminals in both the hippocampus and cerebellum. Furthermore, at the light microscopic level, hippocampal layers that contain the axon arbors of excitatory CA3 pyramidal neurons exhibit the lowest density of axons labeled by the antibody used in the present study in both the rodent (Katona et al., 1999; Hajos et al., 2000) and monkey (Eggan and Lewis, 2007), whereas these layers are densely labeled using the antibody observed to label asymmetric synapses in the rodent (Kawamura et al., 2006; Katona et al., 2006).

Together these data suggest that many of the axon terminals containing both CB1Rs and CCK are likely to arise from a subset of GABA-containing basket neurons that innervate the cell bodies and proximal dendrites of pyramidal neurons. This interpretation is supported by the dual-label immunofluorescence data demonstrating that CB1R/CCK-containing terminals frequently surrounded the perisomatic region of cells. It might be argued that the small percentage of synapses onto somata observed by electron microscopy is inconsistent with this idea since, in the hippocampus, up to 70–80% of terminals from basket neurons target the perisomatic region [defined as the axon initial segment, soma and the first 100 μm of proximal dendrites (see (Freund and Katona, 2007)]. However, in the neocortex this region receives only 20–30% of basket cell synapses (Kisvarday et al., 1985; Freund and

Katona, 2007), and electron microscopic reconstructions of cortical basket cells revealed that 35–50% of their synapses target dendritic shafts (Kisvarday et al., 1985). Furthermore, in the monkey and rodent neocortex the number of small, bipolar, presumably dendrite-targeting CCK neurons outnumber large, multipolar, CCK basket neurons (Hendry et al., 1983; Kubota and Kawaguchi, 1997), and the terminals of calbindin-positive, CCK-negative neurons, some of which express CB1R (Bodor et al., 2005), primarily target dendrites (Kawaguchi and Kubota, 1998; Zaitsev et al., 2005). Thus, given that we analyzed the targets of all CB1R- and CCK-IR terminals, independent of their neurons of origin, the percentage of synapses onto somata and dendrites would be expected to be less than 20% and greater than 50%, respectively, compared to the expected results if only synapses from basket neurons had been analyzed. Therefore, the frequency of synaptic targets reported in this study is consistent with the idea that axon terminals containing both CB1Rs and CCK arise from basket interneurons.

Functional Significance

Perisomatic inputs from CB1R-containing basket neurons are positioned to powerfully regulate pyramidal neuron output by suppressing presynaptic GABA release and reducing $GABA_A$ receptor-mediated inhibitory postsynaptic currents in pyramidal neurons (Trettel et al., 2004; Galarreta et al., 2004; Bodor et al., 2005). Thus, these data suggest a mechanism by which inhibition from CB1R/CCK-IR neurons may serve to regulate network activity that supports working memory. In the rodent neocortex, CB1R/CCK-containing neurons are chemically and electrically coupled (Galarreta et al., 2004) and entrain oscillatory patterns of rhythmic activity (Klausberger et al., 2005; Robbe et al., 2006). Furthermore, the application of CB1R agonists disrupts the power of gamma oscillations in the hippocampus, entorhinal cortex, and prefrontal cortex following administration of CB1R agonists, presumably by disrupting the synchronous firing of pyramidal neurons (Robbe et al., 2006; Hajos et al., 2008). Recent evidence suggests that CB1R/CCK-containing neurons regulate the activity of PV-containing neurons (Foldy et al., 2007; Karson et al., 2008; Karson et al., 2009), which also provide perisomatic inputs to pyramidal cells and play an integral role in entraining gamma oscillations (Lewis et al., 2005); thus, CB1R/CCK-IR neurons may regulate gamma oscillations by acting as a molecular switch that can determine the source and strength of perisomatic inhibition onto pyramidal cells (Foldy et al., 2007). In the human DLPFC, the power of gamma band ocillations increases with, and in proportion to, increasing working memory load (Howard et al., 2003). Therefore, the ability of CB1R activation to disrupt gamma oscillations may be a contributing mechanism by which the systemic administration of cannabinoids disrupts the ability to perform working memory tasks in both humans and animals (Winsauer et al., 1999; Schneider and Koch, 2003; D'Souza et al., 2004).

Cortical pyramidal neurons receive convergent perisomatic input from PV-containing basket and chandelier neurons and CB1R/CCK-containing basket neurons. In the hippocampus these convergent sources of perisomatic inhibition play specific roles in shaping network activity. For example, CB1R/CCK-containing and PV-containing neurons fire at different phases of network oscillations (Klausberger et al., 2005), generate temporally distinct epochs of somatic inhibition (Glickfeld and Scanziani, 2006), and play complementary roles in regulating gamma band oscillations (Hajos et al., 2000). In the monkey DLPFC, markers of the functional properties of PV-containing neurons undergo substantial changes during postnatal development, especially during adolescence (Cruz et al., 2003), that are thought to reflect maturational changes in the regulation of pyramidal cell output. Because stimulation of the CB1R strongly suppresses GABA input to pyramidal neurons from CCK-containing basket neurons, cannabis use during adolescence may alter the balance between the CB1R/CCK-containing and PV-containing inhibitory inputs to the perisomatic region of DLPFC

pyramidal neurons (Foldy et al., 2007; Karson et al., 2008; Karson et al., 2009). This imbalance during a sensitive period may disrupt the developmental trajectories of these GABA inputs (Chattopadhyaya et al., 2007), perhaps through the activity-dependent stimulation of the mammalian target of rapamycin (mTOR) pathway, which is known to induce the translation of proteins involved in neuronal development and long-term modification of synaptic strength and that has recently been demonstrated to be induced by CB1R activation (Puighermanal et al., 2009). Thus, over activation of CB1R by exogenous cannabinoids could produce persistent circuitry alterations that impair the mechanisms of neural synchrony required for the maturation of working memory performance, and perhaps explaining why cannabis use during adolescence is associated with an increased liability for schizophrenia (Murray et al., 2007).

Supplementary Material

Refer to Web version on PubMed Central for supplementary material.

Acknowledgments

The authors wish to thank Dr. Ken Mackie for kindly donating the CB1R antibodies, Nestor Barrezueta for kindly providing CB1R heterozygous and knockout mice brains, and Mary Brady for assistance with the graphics. This work was supported by National Institutes of Health grant number MH051234, the Andrew Mellon Predoctoral Fellowship (SME) and the Scottish Rite Fellowship (SME).

ABBREVIATIONS

CB1R	Cannabinoid 1 receptor
CCK	Cholecystokinin
CR	Calretinin
DAB	3,3′-diaminobenzidine
df	Degrees of freedom
DLPFC	Dorsolateral prefrontal cortex
GABA	γ-aminobutyric acid
IR	Immunoreactive
NDS	Normal donkey serum
NGS	Normal goat serum
NHuS	Normal human serum
PB	Phosphate buffer
PBS	Phosphate buffered saline
PV	Parvalbumin
RT	Room temperature
χ^2	Chi Square

References

Bacci A, Huguenard JR, Prince DA. Long-lasting self-inhibition of neocortical interneurons mediated by endocannabinoids. Nature. 2004; 431:312–316. [PubMed: 15372034]

Bodor AL, Katona I, Nyiri G, Mackie K, Ledent C, Hajos N, Freund TF. Endocannabinoid signaling in rat somatosensory cortex: laminar differences and involvement of specific interneuron types. J Neurosci. 2005; 25:6845–6856. [PubMed: 16033894]

Celio MR, Baier W, Schärer L, de Viragh PA, Gerday Ch. Monoclonal antibodies directed against the calcium binding protein parvalbumin. Cell Calcium. 1988; 9:81–86. [PubMed: 3383226]

Chattopadhyaya B, Di Cristo G, Wu CZ, Knott G, Kuhlman S, Fu Y, Palmiter RD, Huang ZJ. GAD67-mediated GABA synthesis and signaling regulate inhibitory synaptic innervation in the visual cortex. Neuron. 2007; 54:889–903. [PubMed: 17582330]

Connors BW, Long MA. Electrical synapses in the mammalian brain. Annu Rev Neurosci. 2004; 27:393–418. [PubMed: 15217338]

Cruz DA, Eggan SM, Lewis DA. Postnatal development of pre- and post-synaptic GABA markers at chandelier cell inputs to pyramidal neurons in monkey prefrontal cortex. J Comp Neurol. 2003; 465:385–400. [PubMed: 12966563]

D'Souza DC, Perry E, MacDougall L, Ammerman Y, Cooper T, Wu YT, Braley G, Gueorguieva R, Krystal JH. The psychotomimetic effects of intravenous delta-9-tetrahydrocannabinol in healthy individuals: implications for psychosis. Neuropsychopharm. 2004; 29:1558–1572.

DeFelipe J, González-Albo MC, del Río MR, Elston GN. Distribution and patterns of connectivity of interneurons containing calbindin, calretinin, and parvalbumin in visual areas of the occipital and temporal lobes of the macaque monkey. J Comp Neurol. 1999; 412:515–526. [PubMed: 10441237]

Egertová M, Elphick MR. Localisation of cannabinoid receptors in the rat brain using antibodies to the intracellular C-terminal tail of CB. J Comp Neurol. 2000; 422:159–171. [PubMed: 10842224]

Eggan SM, Hashimoto T, Lewis DA. Reduced cortical cannabinoid 1 receptor messenger RNA and protein expression in schizophrenia. Arch Gen Psychiatry. 2008; 65:772–784. [PubMed: 18606950]

Eggan SM, Lewis DA. Immunocytochemical distribution of the cannabinoid CB1 receptor in the primate neocortex: a regional and laminar analysis. Cereb Cortex. 2007; 17:175–191. [PubMed: 16467563]

Foldy C, Lee SY, Szabadics J, Neu A, Soltesz I. Cell type-specific gating of perisomatic inhibition by cholecystokinin. Nat Neurosci. 2007; 10:1128–1130. [PubMed: 17676058]

Freund TF, Katona I. Perisomatic inhibition. Neuron. 2007; 56:33–42. [PubMed: 17920013]

Freund TF, Katona I, Piomelli D. Role of endogenous cannabinoids in synaptic signaling. Physiol Rev. 2003; 83:1017–1066. [PubMed: 12843414]

Galarreta M, Erdelyi F, Szabo G, Hestrin S. Electrical coupling among irregular-spiking GABAergic interneurons expressing cannabinoid receptors. J Neurosci. 2004; 24:9770–9778. [PubMed: 15525762]

Geola FL, Hershman JM, Warwick R, Reeve JR, Walsh JH, Tourtellotte WW. Regional distribution of cholecystokinin-like immunoreactivity in the human brain. J Clin Endocrinol Metab. 1981; 53:270–275. [PubMed: 6265485]

Glass M, Dragunow M, Faull RL. Cannabinoid receptors in the human brain: a detailed anatomical and quantitative autoradiographic study in the fetal, neonatal and adult human brain. Neuroscience. 1997; 77:299–318. [PubMed: 9472392]

Glickfeld LL, Scanziani M. Distinct timing in the activity of cannabinoid-sensitive and cannabinoid-insensitive basket cells. Nat Neurosci. 2006; 9:807–815. [PubMed: 16648849]

Goldman-Rakic PS. Cellular basis of working memory. Neuron. 1995; 14:477–485. [PubMed: 7695894]

Hajos M, Hoffmann WE, Kocsis B. Activation of cannabinoid-1 receptors disrupts sensory gating and neuronal oscillation: relevance to schizophrenia. Biol Psychiatry. 2008; 63:1075–1083. [PubMed: 18261715]

Hajos N, Katona I, Naiem SS, Mackie K, Ledent C, Mody I, Freund TF. Cannabinoids inhibit hippocampal GABAergic transmission and network oscillations. Eur J Neurosci. 2000; 12:3239–3249. [PubMed: 10998107]

Haller J, Matyas F, Soproni K, Varga B, Barsy B, Nemeth B, Mikics E, Freund TF, Hajos N. Correlated species differences in the effects of cannabinoid ligands on anxiety and on GABAergic

and glutamatergic synaptic transmission. Eur J Neurosci. 2007; 25:2445–2456. [PubMed: 17445240]

Hashimoto T, Arion D, Unger T, Maldonado-Aviles JG, Morris HM, Volk DW, Mirnics K, Lewis DA. Alterations in GABA-related transcriptome in the dorsolateral prefrontal cortex of subjects with schizophrenia. Mol Psychiatry. 2008; 13:147–161. [PubMed: 17471287]

Hefft S, Jonas P. Asynchronous GABA release generates long-lasting inhibition at a hippocampal interneuron-principal neuron synapse. Nat Neurosci. 2005; 8:1319–1328. [PubMed: 16158066]

Hendry SHC, Jones EG, Beinfeld MC. Cholecystokinin-immunoreactive neurons in rat and monkey cerebral cortex make symmetric synapses and have intimate associations with blood vessels. Proc Natl Acad Sci USA. 1983; 80:2400–2404. [PubMed: 6132387]

Henquet C, Krabbendam L, Spauwen J, Kaplan C, Lieb R, Wittchen HU, van Os J. Prospective cohort study of cannabis use, predisposition for psychosis, and psychotic symptoms in young people. BMJ. 2005; 330:11–16. [PubMed: 15574485]

Howard MW, Rizzuto DS, Caplan JB, Madsen JR, Lisman J, Aschenbrenner-Scheibe R, Schulze-Bonhage A, Kahana MJ. Gamma oscillations correlate with working memory load in humans. Cereb Cortex. 2003; 13:1369–1374. [PubMed: 14615302]

Hsu S-M, Raine L, Fanger H. Use of avidin-biotin-peroxidase complex (ABC) in immunoperoxidase techniques: A comparison between ABC and unlabeled antibody (PAP) procedures. J Histochem Cytochem. 1981; 29:577–580. [PubMed: 6166661]

Hungund BL, Basavarajappa BS. Distinct differences in the cannabinoid receptor binding in the brain of C57BL/6 and DBA/2 mice, selected for their differences in voluntary ethanol consumption. J Neurosci Res. 2000; 60:122–128. [PubMed: 10723075]

Karson MA, Tang AH, Milner TA, Alger BE. Synaptic cross talk between perisomatic-targeting interneuron classes expressing cholecystokinin and parvalbumin in hippocampus. J Neurosci. 2009; 29:4140–4154. [PubMed: 19339609]

Karson MA, Whittington KC, Alger BE. Cholecystokinin inhibits endocannabinoid-sensitive hippocampal IPSPs and stimulates others. Neuropharmacology. 2008; 54:117–128. [PubMed: 17689570]

Katona I, Sperlagh B, Sik A, Kafalvi A, Vizi ES, Mackie K, Freund TF. Presynaptically located CB1 cannabinoid receptors regulate GABA release from axon terminals of specific hippocampal interneurons. J Neurosci. 1999; 19:4544–4558. [PubMed: 10341254]

Katona I, Urban GM, Wallace M, Ledent C, Jung KM, Piomelli D, Mackie K, Freund TF. Molecular composition of the endocannabinoid system at glutamatergic synapses. J Neurosci. 2006; 26:5628–5637. [PubMed: 16723519]

Kawaguchi Y, Kubota Y. Neurochemical features and synaptic connections of large physiologically-identified GABAergic cells in the rat frontal cortex. Neuroscience. 1998; 85:677–701. [PubMed: 9639265]

Kawamura Y, Fukaya M, Maejima T, Yoshida T, Miura E, Watanabe M, Ohno-Shosaku T, Kano M. The CB1 cannabinoid receptor is the major cannabinoid receptor at excitatory presynaptic sites in the hippocampus and cerebellum. J Neurosci. 2006; 26:2991–3001. [PubMed: 16540577]

Kisvarday ZF, Martin KA, Whitteridge D, Somogyi P. Synaptic connections of intracellularly filled clutch cells: a type of small basket cell in the visual cortex of the cat. J Comp Neurol. 1985; 241:111–137. [PubMed: 4067011]

Klausberger T, Marton LF, O'Neill J, Huck JH, Dalezios Y, Fuentealba P, Suen WY, Papp E, Kaneko T, Watanabe M, Csicsvari J, Somogyi P. Complementary roles of cholecystokinin- and parvalbumin-expressing GABAergic neurons in hippocampal network oscillations. J Neurosci. 2005; 25:9782–9793. [PubMed: 16237182]

Kovacs TO, Walsh JH, Maxwell V, Wong HC, Azuma T, Katt E. Gastrin is a major mediator of the gastric phase of acid secretion in dogs: proof by monoclonal antibody neutralization. Gastroenterology. 1989; 97:1406–1413. [PubMed: 2583408]

Kubota Y, Kawaguchi Y. Two distinct subgroups of cholecystokinin-immunoreactive cortical interneurons. Brain Res. 1997; 752:175–183. [PubMed: 9106454]

Lewis DA, Campbell MJ, Morrison JH. An immunohistochemical characterization of somatostatin-28 and somatostatin-28 (1–12) in monkey prefrontal cortex. J Comp Neurol. 1986; 248:1–18. [PubMed: 2873154]

Lewis DA, Hashimoto T, Volk DW. Cortical inhibitory neurons and schizophrenia. Nat Rev Neurosci. 2005; 6:312–324. [PubMed: 15803162]

Lund JS, Lewis DA. Local circuit neurons of developing and mature macaque prefrontal cortex: Golgi and immunocytochemical characteristics. J Comp Neurol. 1993; 328:282–312. [PubMed: 7678612]

Marsicano G, Lutz B. Expression of the cannabinoid receptor CB1 in distinct neuronal subpopulations in the adult mouse forebrain. Eur J Neurosci. 1999; 11:4213–4225. [PubMed: 10594647]

McGuire BA, Gilbert CD, Rivlin PK, Wiesel TN. Targets of horizontal connections in macaque primary visual cortex. J Comp Neurol. 1991; 305:370–392. [PubMed: 1709953]

Melchitzky DS, Eggan SM, Lewis DA. Synaptic targets of calretinin-containing axon terminals in macaque monkey prefrontal cortex. Neuroscience. 2005; 130:185–195. [PubMed: 15561434]

Moore TH, Zammit S, Lingford-Hughes A, Barnes TR, Jones PB, Burke M, Lewis G. Cannabis use and risk of psychotic or affective mental health outcomes: a systematic review. Lancet. 2007; 370:319–328. [PubMed: 17662880]

Murray RM, Morrison PD, Henquet C, Di Forti M. Cannabis, the mind and society: the hash realities. Nat Rev Neurosci. 2007; 8:885–895. [PubMed: 17925811]

Oeth KM, Lewis DA. Cholecystokinin innervation of monkey prefrontal cortex: An immunohistochemical study. J Comp Neurol. 1990; 301:123–137. [PubMed: 1706355]

Oeth KM, Lewis DA. Postnatal development of the cholecystokinin innervation of monkey prefrontal cortex. J Comp Neurol. 1993; 336:400–418. [PubMed: 8263229]

Peters, A.; Palay, SL.; Webster, DF. The fine structure of the nervous system. New York: Oxford University Press; 1991.

Puighermanal E, Marsicano G, Busquets-Garcia A, Lutz B, Maldonado R, Ozaita A. Cannabinoid modulation of hippocampal long-term memory is mediated by mTOR signaling. Nat Neurosci. 2009; 12:1152–1158. [PubMed: 19648913]

Rao SG, Williams GV, Goldman-Rakic PS. Destruction and creation of spatial tuning by disinhibition: $GABA_A$ blockade of prefrontal cortical neurons engaged by working memory. J Neurosci. 2000; 20:485–494. [PubMed: 10627624]

Rehfeld JF. Localisation of gastrins to neuro- and adenohypophysis. Nature. 1978; 271:771–773. [PubMed: 625350]

Robbe D, Montgomery SM, Thome A, Rueda-Orozco PE, McNaughton BL, Buzsaki G. Cannabinoids reveal importance of spike timing coordination in hippocampal function. Nat Neurosci. 2006; 9:1526–1533. [PubMed: 17115043]

Saper CB. An open letter to our readers on the use of antibodies. J Comp Neurol. 2005; 493:477–478. [PubMed: 16304632]

Saper CB, Sawchenko PE. Magic peptides, magic antibodies: guidelines for appropriate controls for immunohistochemistry. J Comp Neurol. 2003; 465:161–163. [PubMed: 12949777]

Sawaguchi T, Matsumura M, Kubota K. Delayed response deficit in monkeys by locally disturbed prefrontal neuronal activity by bicuculline. Behav Brain Res. 1988; 31:193–198. [PubMed: 2849457]

Schneider M, Koch M. Chronic pubertal, but not adult chronic cannabinoid treatment impairs sensorimotor gating, recognition memory, and the performance in a progressive ratio task in adult rats. Neuropsychopharmacology. 2003; 28:1760–1769. [PubMed: 12888772]

Sesack SR, Hawrylak VA, Matus C, Guido MA, Levey AI. Dopamine axon varicosities in the prelimbic division of the rat prefrontal cortex exhibit sparse immunoreactivity for the dopamine transporter. J Neurosci. 1998; 18:2697–2708. [PubMed: 9502827]

Sesack SR, Snyder CL, Lewis DA. Axon terminals immunolabeled for dopamine or tyrosine-hydroxylase synapse on GABA-immunoreactive dendrites in rat and monkey cortex. J Comp Neurol. 1995; 363:264–280. [PubMed: 8642074]

Smiley JF, Goldman-Rakic PS. Heterogeneous targets of dopamine synapses in monkey prefrontal cortex demonstrated by serial section electron microscopy: A laminar analysis using the silver-

enhanced diaminobenzidine sulfide (SEDS) immunolabeling technique. Cereb Cortex. 1993; 3:223–238. [PubMed: 7686795]

Trettel J, Fortin DA, Levine ES. Endocannabinoid signalling selectively targets perisomatic inhibitory inputs to pyramidal neurones in juvenile mouse neocortex. J Physiol. 2004; 556:95–107. [PubMed: 14742727]

Winsauer PJ, Lambert P, Moerschbaecher JM. Cannabinoid ligands and their effects on learning and performance in rhesus monkeys. Behav Pharmacol. 1999; 10:497–511. [PubMed: 10780256]

Zaitsev AV, Gonzalez-Burgos G, Povysheva NV, Kroner S, Lewis DA, Krimer LS. Localization of calcium-binding proteins in physiologically and morphologically characterized interneurons of monkey dorsolateral prefrontal cortex. Cereb Cortex. 2005; 15:1178–1186. [PubMed: 15590911]

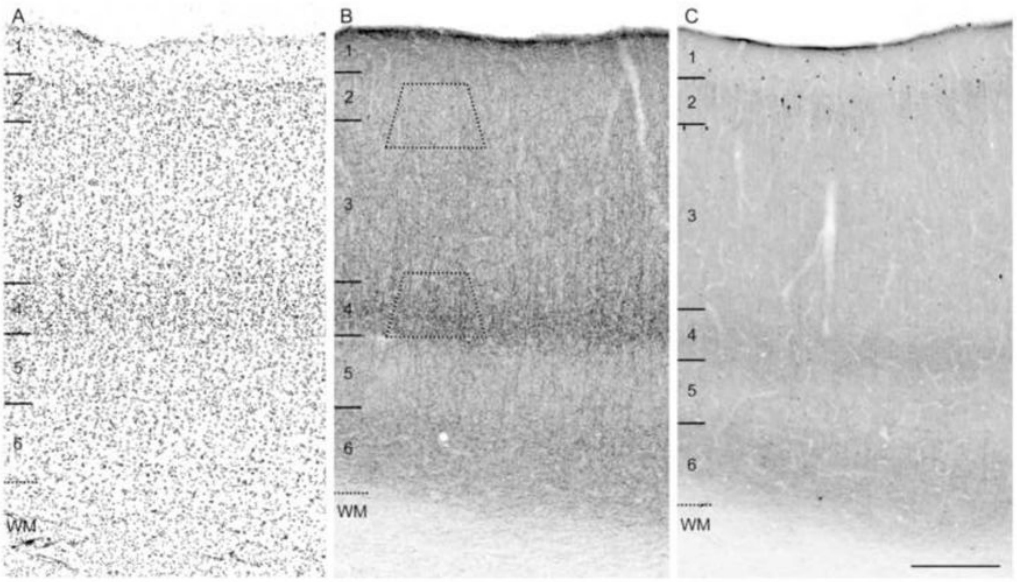

Figure 1.

Brightfield photomicrographs of immunoreactivity produced by the guinea pig anti-CB1R and mouse anti-CCK antibodies in area 46 of monkey DLPFC. Both CB1R (B) and CCK (C) antibodies labeled numerous fibers that were thin, rich in varicosities, and distributed with similar laminar patterns. Both CB1R and CCK-labeled neurons were most frequently present in layers 2 and superficial 3 (B, C). In panels A, B, and C numbers and hash marks to the left indicate the positions of the cortical layers, and the dashed lines denote the layer 6-white matter (WM) border determined from adjacent Nissl sections (A). The trapezoids in panel B show the approximate laminar location of blocks examined for electron microscopy. Scale bar = 300 μm and applies to all panels.

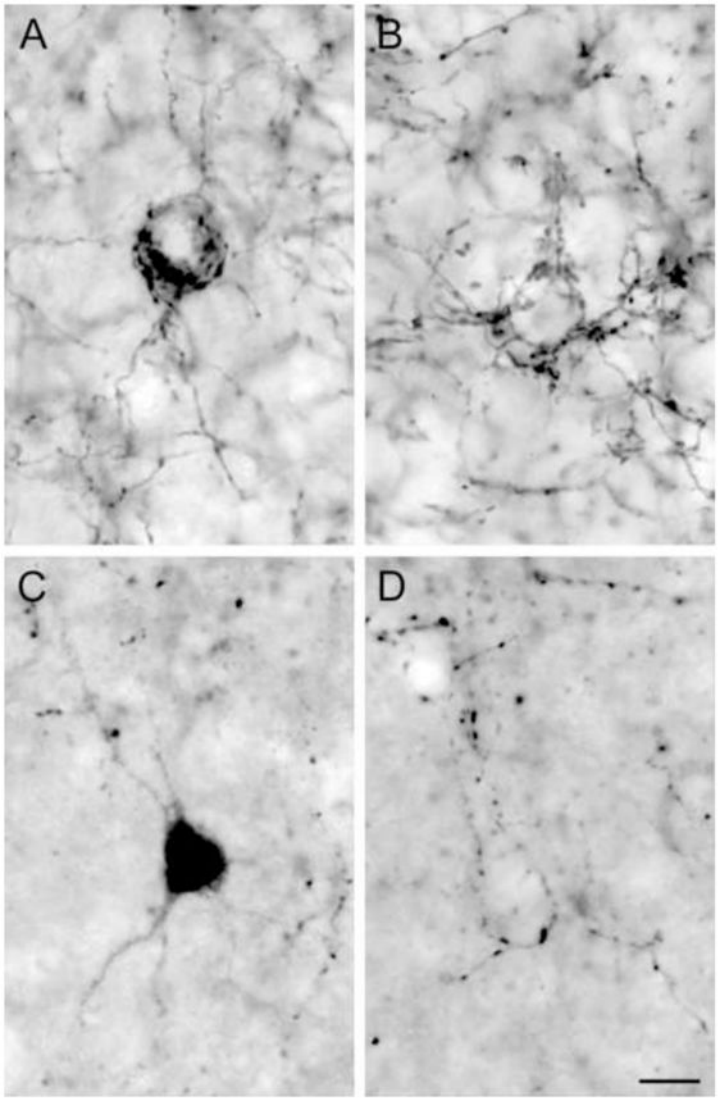

Figure 2.

Morphology and distinct innervation pattern CB1R and CCK-IR neurons and axon terminals. CB1R- (A) and CCK-IR (C) neurons were often large and multipolar in shape. Some CB1R- (B) and CCK-IR (D) axons formed “baskets” surrounding unlabeled cell bodies. Cells in A and C and “baskets” in B and D were located in layers 2-superficial 3. Scale bar = 10 μm and applies to all panels.

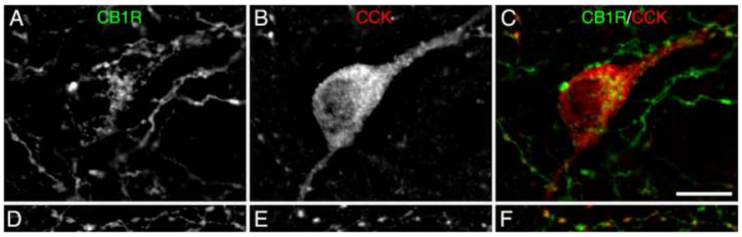

Figure 3.

Fluorescent photomicrographs of CB1R and CCK immunoreactivity in area 46 of monkey DLPFC. (A) CB1R-IR neuron labeled with Alexa 488 (green). (B) CCK-IR neuron labeled with Cy3 (red). (C) Overlay of panels A and B showing the colocalization (yellow) of CB1R and CCK in the same cell. (D) CB1R-IR axon and varicosities labeled with Alexa 488 (green). (E) axon and varicosities labeled with Cy3 (red). (F) Overlay of panels D and E showing the colocalization (yellow) of CB1R and CCK in the same axon and varicosities. Scale bar = 10 μm and applies to all panels.

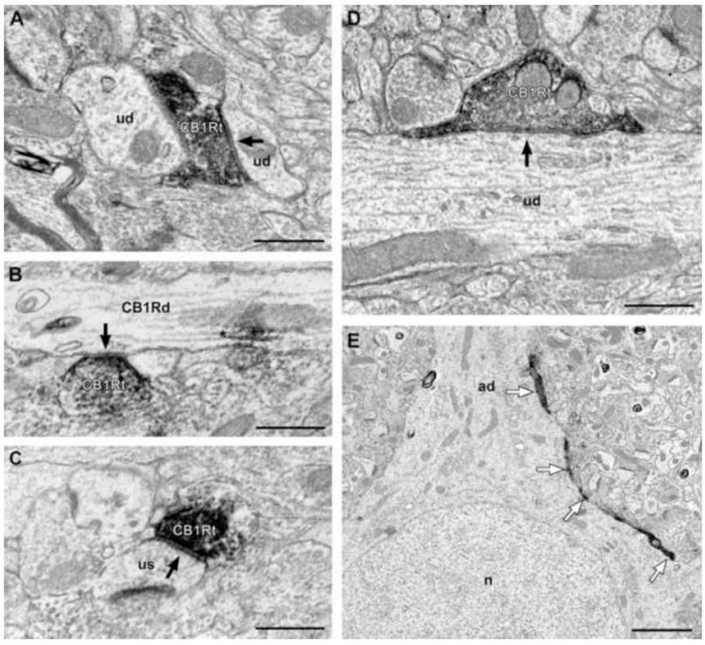

Figure 4.

Electron micrographs of CB1R-IR axon terminals forming symmetric synapses in area 46 of monkey DLPFC. CB1R-IR axon terminals (CB1Rt) form symmetric synapses (arrows) onto small (A) and large (D) unlabeled dendritic shafts (ud). (B) CB1Rt forms a symmetric synapse (arrow) onto a CB1R-IR dendritic shaft (CB1Rd). Reaction product in dendrites (asterisk) was associated with microtubules. (C) A CB1t forms a symmetric synapse onto an unlabeled dendritic spine (us). (E) Low power electron micrograph demonstrating a CB1R-IR axon forming “basket-like” appositions (white arrows) around an unlabeled cell body (ad = apical dendrite, n = nucleus). Scale bars = 500 nm in A-D and 2 μm in E.

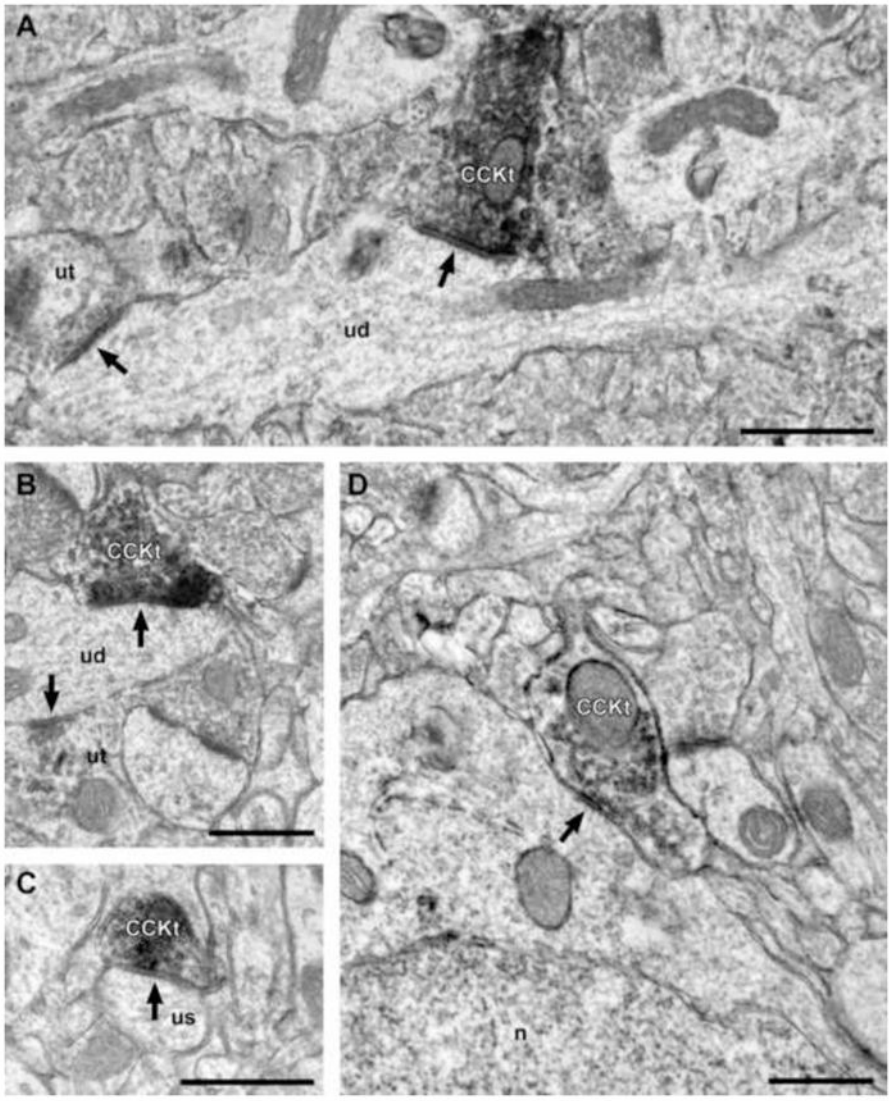

Figure 5.

Electron micrographs of CCK-IR axon terminals forming symmetric synapses in area 46 of monkey DLPFC. (A, B) A CCK-IR axon terminal (CCKt) forms a symmetric synapse (arrow) onto an unlabeled dendritic shaft (ud). Note that the dendritic shafts are varicose in shape and receive a synaptic input from another, unlabeled axon terminal (ut; arrow), which are morphologic characteristics of GABA neuron dendrites. (C) A CCKt forms a symmetric synapse onto a dendritic unlabeled spine (us). (D) A CCKt forms a symmetric synapse (arrow) onto an unlabeled soma (n = nucleus). Scale bars = 500 nm in all panels.

Table 1

Comparison of the synaptic targets of CB1R- and CCK-IR axon terminals forming symmetric synapses in layers 2-superficial 3 and layer 4 of monkey DLPFC area 46.

	Dendritic Shafts	Somata	Dendritic Spines	Statistical Results
Layers 2-superficial 3				
Number (%) of CB1R-IR axon terminals	49 (88%)	0 (0%)	7 (12%)	$\chi^2 = 6.93$ $p = 0.031$
Number (%) of CCK-IR axon terminals	21 (81%)	3 (11%)	2 (8%)	
Layer 4				
Number (%) CB1R-IR axon terminals	48 (87%)	2 (4%)	5 (9%)	$\chi^2 = 0.56$ $p = 0.755$
Number (%) CCK-IR axon terminals	48 (83%)	2 (3%)	8 (14%)	